CANCER

Cell type–dependent bimodal p53 activation engenders a dynamic mechanism of chemoresistance

Ruizhen Yang[1]*, Bo Huang[1,2]*, Yanting Zhu[1], Yang Li[1], Feng Liu[2†], Jue Shi[1†]

Copyright © 2018 The Authors, some rights reserved; exclusive licensee American Association for the Advancement of Science. No claim to original U.S. Government Works. Distributed under a Creative Commons Attribution NonCommercial License 4.0 (CC BY-NC).

Studies of drug resistance mostly characterize genetic mutation, and we know much less about phenotypic mechanisms of drug resistance, especially at a quantitative level. p53 is an important mediator of cellular response to chemotherapy, but even p53 wild-type cells vary in drug sensitivity for unclear reasons. Here, we elucidated a new resistance mechanism to a DNA-damaging chemotherapeutic through bimodal modulation of p53 activation dynamics. By combining single-cell imaging with computational modeling, we characterized a four-component regulatory module, which generates bimodal p53 dynamics through coupled feed-forward and feedback, and found that the inhibitory strength between ATM and Mdm2 determined the differential modular output between drug-sensitive and drug-resistant cancer cell lines. We further showed that the combinatorial inhibition of Mdm2 and Wip1 was an effective strategy to alter p53 dynamics in resistant cancer cells and sensitize their apoptotic response. Our results point to p53 pulsing as a potentially druggable mechanism that mediates chemoresistance.

INTRODUCTION

Tumors exhibit large intrinsic variation in drug responsiveness due to both intratumoral and intertumoral heterogeneity; previously sensitive tumors commonly evolve to be drug resistant during chemotherapy. To improve therapy, we need better understanding of both intrinsic and acquired drug resistance. Most well-known mechanisms of drug resistance involve genetic mutation, such as mutation of target genes of kinase inhibitors and mutation of genes that mediate drug responses, e.g., p53 for DNA-damaging drugs (*1*, *2*). However, for most commonly used cytotoxic chemotherapy, the mechanistic basis of drug sensitivity is unclear at both genotype and phenotype levels.

The p53 pathway, consisting of the tumor suppressor protein p53, its upstream regulators, and downstream target genes, plays a central role in mediating cellular response to chemotherapeutics (*3*–*5*). Loss of p53 function due to p53 mutation has been widely studied with respect to chemoresistance. However, drug resistance is also often seen, and may be even greater, in tumors with wild-type p53 (*6*–*8*). Extensive biochemical and cell biology studies have revealed that p53 activity is regulated by multiple posttranslational modifications (*9*, *10*), differential subcellular localization (*11*), and interaction with cofactors (*12*). Drug resistance may arise from all of these venues. More recently, single-cell studies both by us and others showed that alteration of the activation dynamics of p53 is another mechanism to modulate p53 activity in response to DNA-damaging drugs, raising the interesting possibility of a mechanistic link between p53 activation dynamics and drug sensitivity (*13*, *14*).

The control of p53 dynamics in response to DNA damage was first examined for transient γ-radiation or ultraviolet (UV) radiation and revealed intriguing oscillation of p53 levels that culminated in mostly cell cycle arrest and senescence, but not cell death (*15*–*18*). In a recent study of a cancer cell line panel, p53 dynamics were found to vary substantially between cell lines (*19*). Nonetheless, despite the difference in p53 activation dynamics, cell cycle arrest was the primary damage response phenotype for all cell types. The lack of differential cellular response, in particular cell death response, in these previous studies was probably due to the low level of DNA damage used. By examining a much larger dose range of DNA damage triggered by a DNA-damaging chemotherapeutic, etoposide, we uncovered a new dynamical regime of p53 activation at high DNA damage, i.e., monotonic induction, which specifically led to apoptosis (*13*). We further showed that changing p53 dynamics from oscillation to monotonic increase was sufficient to switch cellular response from cell cycle arrest to apoptosis in drug-sensitive cell lines. However, the above studies left unexplained the role of p53 dynamics in drug resistance, in particular resistance to drug-induced cell death.

We thus set out to investigate p53 activation dynamics of a panel of cancer cell lines that showed variable sensitivity to a DNA-damaging drug. We observed cell type–dependent bimodal regulation of p53 that correlated with sensitivity to drug-induced apoptosis. In cell lines sensitive to etoposide, p53 switched from oscillation to strong monotonic induction followed by rapid cell death, as etoposide concentration increased. In contrast, p53 switched to a dynamic mode of extended large pulse in the drug-resistant cell lines and triggered mostly cell cycle arrest, not cell death. To unravel the mechanistic basis underlying the observed cell type variation in p53 dynamics and its role in chemoresistance, we combined quantitative single-cell imaging with mathematical modeling. Our results elucidated a four-component regulatory module involving ATM, p53, Mdm2, and Wip1, which activates p53 dynamics and drug response in a dose-dependent and cell type–dependent manner through coupled feed-forward and feedback. Our data also revealed combinatorial perturbation that can revert drug resistance and could be developed into a therapeutic strategy.

RESULTS

Cell type variation in p53 dynamics and cellular response

Etoposide induces DNA double-stranded breaks by inhibiting topoisomerase II and is a DNA-damaging chemotherapeutic commonly used in the clinic (*20*). We focused our study on etoposide, as it acts mainly through p53-mediated DNA damage response (fig. S1). We first compared the dose response of etoposide-sensitive (A375, U-2 OS, and A549) and etoposide-resistant cell lines (MCF7, HepG2, and 769-P) that harbor wild-type p53, as well as their respective drug-induced p53 dynamics. To monitor real-time p53 dynamics in individual cells,

[1]Center for Quantitative Systems Biology, Department of Physics and Department of Biology, Hong Kong Baptist University, Hong Kong, China. [2]National Laboratory of Solid State Microstructures, Department of Physics and Collaborative Innovation Center of Advanced Microstructure, Nanjing University, Nanjing, China.
*These authors contributed equally to this work.
†Corresponding author. Email: jshi@hkbu.edu.hk (J.S.); fliu@nju.edu.cn (F.L.)

we used clonal fluorescent reporter cell lines that stably express a p53-Venus construct (*13*). Dynamics of the p53-Venus construct have been confirmed to behave similarly to its wild-type counterpart (*13*, *15*). Time-lapse imaging of the fluorescent reporter lines showed that upon drug treatment, the fluorescent signal of p53-Venus primarily localized in the nucleus and showed a dose-dependent bimodal regulation (Fig. 1, A and B). At low drug doses (1 to 10 μM), nuclear p53 mostly exhibited periodic pulsing in both the sensitive and resistant cell lines. As etoposide concentration increased, p53 switched from periodic pulsing to two distinct dynamic modes, i.e., monotonic induction in etoposide-sensitive cell lines and an extended large pulse in the resistant lines. Single-cell statistics demonstrated that, although cell-to-cell variability was significant in terms of the timing and p53 induction level, cells within the sensitive lines predominantly showed sustained p53 induction at high drug dose, while p53 level evidently decreased after the initial rise in cells from the resistant lines with periods of 10 to 15 hours, which were about 1.5- to 2-fold longer than the oscillatory period at low drug dose (Fig. 1C and fig. S2). Moreover, the average peak level of p53 induced by high drug concentrations was 7- to 9-fold higher than that by low drug concentrations in the sensitive lines, as compared to a 2- to 5-fold increase in the resistant lines (Fig. 1D). The combination of pulsing dynamics and lower activation amplitudes resulted in a substantially lower integrated level of p53 induction in the resistant cell lines in response to high concentration of etoposide.

We next examined the dose-response phenotype (see Materials and Methods for details) and its correlation with the differential p53 dynamics observed in individual cells. As shown in the top panel of Fig. 1E, >95% of cells from all six cell lines (summed over all drug

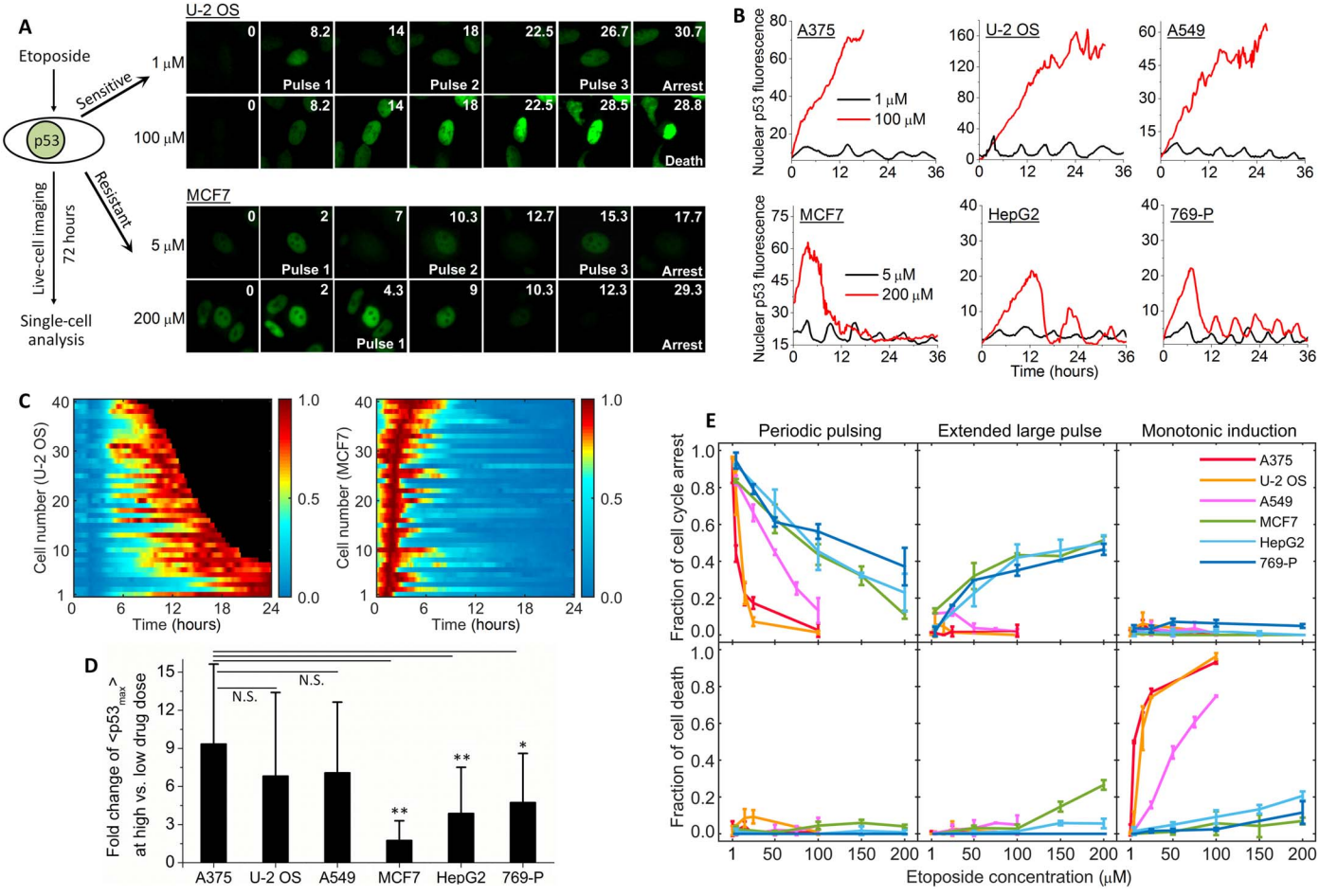

Fig. 1. p53 dynamics and cellular response to etoposide were both dose and cell type dependent. (**A**) p53 dynamics monitored by p53-Venus fluorescence in the representative drug-sensitive cell line U-2 OS (top) and resistant cell line MCF7 (bottom) at low and high concentrations of etoposide. Still images were from time-lapse movies. Time (unit: hour) is indicated at the top right corner of each image. (**B**) Representative single-cell trajectories of p53 dynamics quantified from fluorescence of the p53-Venus reporter in the nucleus of the six cancer cell lines at the indicated low (black lines) and high (red lines) etoposide doses. The abrupt end of p53 trajectories in the sensitive cell lines corresponds to the time of death. (**C**) Heat maps of nuclear p53-Venus fluorescence in U-2 OS (left) and MCF7 cells (right) at high drug dose. Black squares indicate the time of cell death. (**D**) Ratio of the average peak level of p53-Venus fluorescence at high and low drug doses in the six cell lines. Error bars indicate standard deviation (SD). The two-tailed *P* value was obtained by Welch's unpaired *t* test with A375 as the reference group. N.S., not statistically significant. *$P < 0.0003$ and **$P < 0.0001$. (**E**) Fraction of cells that exhibited the three distinct p53 dynamics, i.e., periodic pulsing, an extended large pulse, and a monotonic increase, and went into cell cycle arrest (top) or cell death (bottom) under the indicated etoposide concentration. Data were averaged from two independent sets of single-cell imaging experiments. The total number of cells analyzed for each condition in each imaging experiment ranged from 51 to 143. Error bars indicate SD. The A549 data were replotted from Fig. 2B published in (13) for direct comparison with new data of the other five cell lines.

concentrations) that went into cell cycle arrest showed pulsing dynamics of p53, i.e., either periodic pulsing or an extended large pulse, revealing a strong correlation between pulsing p53 and the response phenotype of cell cycle arrest and survival. As etoptoside concentration increased, both the sensitive and resistant cell lines showed increase of cell death, but the extent of etoposide-induced cell death was significantly less in the resistant lines, i.e., MCF7, HepG2, and 769-P (Fig. 1E, bottom). Seventy-two–hour treatment of 200 μM etoposide only induced less than 36% cell death in the resistant lines, as compared with more than 80% cell death in the three sensitive lines upon treatment of 100 μM etoposide. Moreover, the high level of cell death exhibited by the sensitive lines strongly correlated with the p53 dynamic mode of monotonic increase (Fig. 1E, bottom). Our data thus suggest that resistance of MCF7, HepG2, and 769-P to etoposide-induced cell death may be due to the significantly lower activation level of p53 rendered by the extended large-pulse dynamics of p53, as compared with the strong monotonic induction seen in the sensitive lines (Fig. 1, B to D).

We noted that the extended large-pulse mode of p53 dynamics could lead to the response phenotypes of both cell cycle arrest and cell death. For instance, among MCF cells that showed a large p53 pulse, 80% were found to go into cell cycle arrest, while the other 20% died. This can be attributed to the low induction level of p53 in the large-pulse mode and the resulting low accumulative p53 activity that obviously was not sufficient to cross the threshold for triggering cell death for most of the cells from the resistant cell lines. Although the reporter cell lines are isogenic, the threshold for triggering cell death may still vary between individual cells, e.g., because of stochasticity in gene expression (*21*, *22*). Therefore, cell-to-cell variability in sensitivity to cell death coupled with the intermediate level of p53 induction resulting from an extended p53 pulse likely accounted for p53 inducing alternative cell fate of arrest and death in individual cells. Overall, our results demonstrated the importance of cell type–dependent bimodal p53 dynamics in regulating the sensitivity of distinct cancer cells to DNA-damaging chemotherapeutics, and the single-cell data also pointed to a suppressive role of p53 pulsing in attenuating the p53 induction level and subsequent p53-mediated cell death.

Variable p53 dynamics correlated with phospho-ATM and Mdm2 levels

To identify molecular mechanisms underlying the dose-dependent bimodal regulation of p53 and its cell type dependence, we profiled, by Western blotting, the expression and/or posttranslational modification of key regulators that are known to modulate p53 expression and activity, including ATM, Chk2, Mdm2, and Wip1 (Fig. 2A) (*9*, *23*–*25*). We chose U-2 OS and MCF7 as the representative sensitive and resistant cell lines and compared their cellular responses at one low (i.e., 1 μM etoposide for U-2 OS and 5 μM for MCF7) and one high drug concentration (i.e., 100 μM etoposide for U-2 OS and 200 μM for MCF7), under which cells within the same cell line exhibited one primary p53 dynamic mode, i.e., periodic pulsing at low drug dose and monotonic increase or an extended large pulse at high drug dose.

As shown in Fig. 2 (B and C), for both U-2 OS and MCF7 cells, higher drug concentration induced a higher level of p53, similar to the single-cell imaging data. Among the immediate p53 regulators, we found that the dose-dependent expression of Mdm2 and Wip1, the two main negative regulators and transcriptional target genes of p53, varied significantly between U-2 OS and MCF7. For U-2 OS cells, expressions of both Mdm2 and Wip1 steadily increased over time at low etoposide concentration, but such up-regulation was suppressed under high drug dose (Fig. 2B). Inhibition of the negative feedbacks from Mdm2 and Wip1 likely enabled p53 to accumulate to a high level, resulting in its monotonic rise in U-2 OS cells. MCF7 cells, however, exhibited strong up-regulation of Mdm2 and Wip1 at both low and high drug doses (Fig. 2C), which correlated with the much lower level of p53 induction, especially at high drug concentration. Direct comparison of U-2 OS and MCF7 on the same gel further confirmed the differential expression of Mdm2 and Wip1 in these two cell lines that correlated with their differential responses at high drug dose (Fig. 2D). It also revealed a much lower expression of total ATM and phospho-ATM, but higher basal expression of Wip1, in MCF7 than U-2 OS, which may also contribute to an attenuated p53 induction in MCF7.

To examine whether the above differential expression features are common in the other sensitive and resistant cell lines, we compared levels of ATM, phospho-ATM, Mdm2, and Wip1 under low and high drug doses for all six cell lines. As shown in Fig. 2E and fig. S3, the sensitive lines all expressed substantial levels of ATM and phospho-ATM and exhibited significant attenuation of Mdm2 up-regulation under high drug treatment. In contrast, Mdm2 expression remained strongly induced in all resistant lines at high drug dose. Distinct from MCF7 and HepG2, the resistant line 769-P did not significantly express Wip1 or have a lower level of total ATM or phospho-ATM. These data suggest that the cell line–dependent p53 dynamics and variable drug sensitivity are mainly due to differential Mdm2 up-regulation. Moreover, the level of DNA damage induced by etoposide in the same dynamical regime of p53 (indicated by the γH2A.X signal) was largely similar in the sensitive and resistant lines (Fig. 2E). Therefore, the cell line–dependent drug-induced dynamics of p53 and its regulators were not due to difference in the DNA damage signal, but rather due to the variable activation of the p53 regulatory pathway.

To determine whether the distinct p53 dynamics resulted in differential p53 activity, we also measured the expression of p53 target genes critical for cell fate response, such as p21 (cell cycle arrest gene) and Puma (cell death gene). Both p21 and Puma were more rapidly and strongly up-regulated at high drug dose when p53 induction level was higher (Fig. 2F). In particular, high drug dose increased Puma expression by more than 8-fold in U-2 OS cells, which was evidently sufficient to trigger extensive cell death and switched the primary response phenotype from cell cycle arrest to cell death. In contrast, MCF7 cells exhibited only a 3-fold increase in Puma expression, correlating with the much lower level of cell death activation. These data corroborated the role of differential p53 dynamics in regulating p53 activity and subsequent cell fate response, most likely via modulating p53 induction level.

ATM-mediated Mdm2 degradation accounted for attenuated Mdm2 up-regulation

Given the level and dynamics of Mdm2 correlated with cell type–dependent bimodal p53 dynamics, we next examined the mechanism underlying the dose-dependent up-regulation of Mdm2. Suppression of Mdm2 up-regulation in the sensitive lines at high drug concentration, which was not seen in the resistant lines, could be due to reduced gene transcription or translation or increased protein degradation. We had previously performed quantitative real-time polymerase chain reaction analysis and found no differential transcription of the Mdm2 gene at low versus high DNA damage in U-2 OS cells (*13*), indicating that the posttranscriptional mechanism likely accounted for the dose-dependent Mdm2 expression. Moreover, ATM was observed to promote autodegradation of Mdm2 (*26*), which led us to test whether

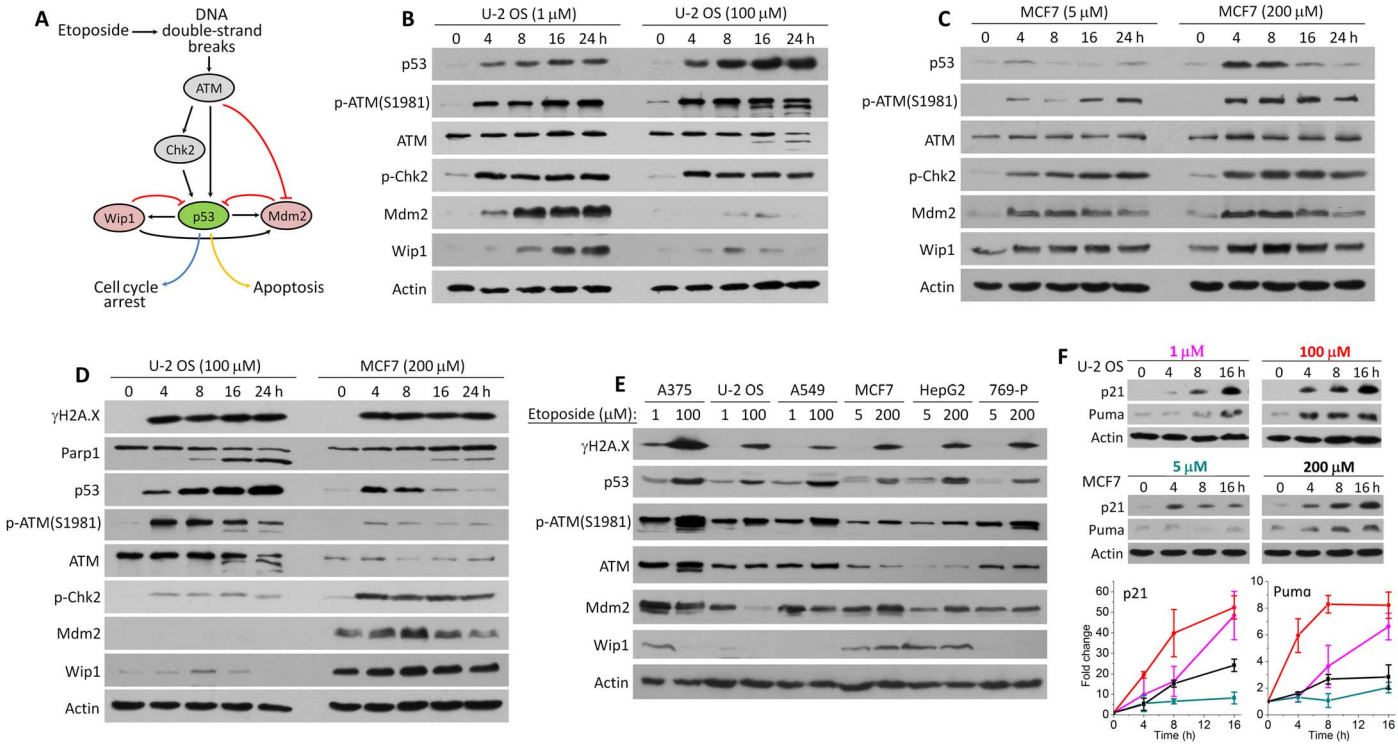

Fig. 2. p53 dynamics and p53-mediated drug response correlated with kinetics of a number of proteins/protein modifications. (**A**) Network diagram of key regulatory components of the p53 pathway associated with response to etoposide. (**B** and **C**) Western blot comparison of dose response of (B) U-2 OS cells and (C) MCF7 cells at low versus high drug concentration. (**D**) Comparison of U-2 OS and MCF7 response at high etoposide concentration. (**E**) Comparison of the six cell lines after an 8-hour treatment of the indicated etoposide concentration. (**F**) Expression of p21 and Puma in U-2 OS and MCF7 at the indicated low versus high etoposide concentration. The quantified Western blot results were color-coded by cell line and drug concentration as indicated. Error bars were SDs calculated on the basis of three independent sets of Western blots. For all Western blotting analysis, actin served as the loading control. DNA damage level was indicated by a DNA damage marker, γH2A.X, and the extent of cell death was indicated by Parp1 cleavage. All data shown are representative of at least three independent Western blot measurements.

the strong elevation of phospho-ATM activity in response to high drug dose triggered more extensive Mdm2 autodegradation, thus restraining Mdm2 expression at a low level. To measure the degradation kinetics of Mdm2 protein, we used cycloheximide to inhibit overall protein translation. For U-2 OS cells, the levels of Mdm2 decreased with a half-life of about 1.96 hours under control condition (no etoposide treatment), 2.02 hours under 1 μM etoposide, and 0.31 hours under 100 μM etoposide (Fig. 3A). That is, the rate of Mdm2 degradation increased by about 6.5-fold at high drug dose as compared with that of low drug dose and control. Moreover, the combinatorial treatment of 100 μM etoposide and 20 μM KU55933, a small-molecule inhibitor of ATM, significantly prolonged the half-life of Mdm2 to 1.16 hours, indicating that the accelerated Mdm2 degradation under high etoposide concentration was mainly mediated by increased ATM activity (Fig. 3A and fig. S4). In contrast, half-life measurement of MCF7 cells revealed only a less than 2-fold decrease of Mdm2 half-life at high drug dose versus low drug dose and control (Fig. 3B), demonstrating that Mdm2 autodegradation was significantly less in MCF7 compared to U-2 OS cells and not sufficient to suppress Mdm2 up-regulation.

Similar characteristics of Mdm2 degradation kinetics were also observed in the other two sensitive and resistant cell lines (Fig. 3C and fig. S5). Hence, our results point to enhanced Mdm2 degradation mediated by increased ATM activity as the key mechanism underlying the attenuation of Mdm2 up-regulation. The combined inhibitory interaction of ATM-Mdm2 and Mdm2-p53 thus formed a double negative, i.e., positive feed-forward control that rendered strong, monotonically increasing p53 in the etoposide-sensitive cell lines in response to high drug dose, and the inhibitory strength of ATM-Mdm2 interaction was significantly attenuated in the resistant cell lines. For MCF7 and HepG2, this can be attributed to the substantially lower level of phospho-ATM (a surrogate of ATM activity), likely resulting from the low expression of total ATM. As for 769-P, the attenuation of ATM-Mdm2 interaction may be due to reduced ATM-Mdm2 binding or reduced ATM activity in catalyzing Mdm2 autodegradation.

Mathematical modeling of p53 dynamics

To quantitatively understand how the feed-forward of ATM-Mdm2-p53, together with or without the negative feedback of Wip1-p53, collectively controls the dose-dependent bimodal p53 dynamics and to investigate cell type differences, we performed a computational analysis. We established a four-component model, consisting of ATM, p53, Mdm2, and Wip1, for the representative cell lines, U-2 OS (sensitive) and MCF7 (resistant) (Fig. 4, A and B). We implemented a standard negative feedback between p53 and Mdm2, and both p53 and Mdm2 can be phosphorylated by ATM and dephosphorylated by Wip1. As Wip1 is also a transcriptional target of p53, a second negative feedback was defined between p53 and Wip1. Moreover, the phosphorylation of Mdm2 by ATM attenuates its inhibition of p53 and also promotes its autodegradation, thus forming a feed-forward between ATM, Mdm2,

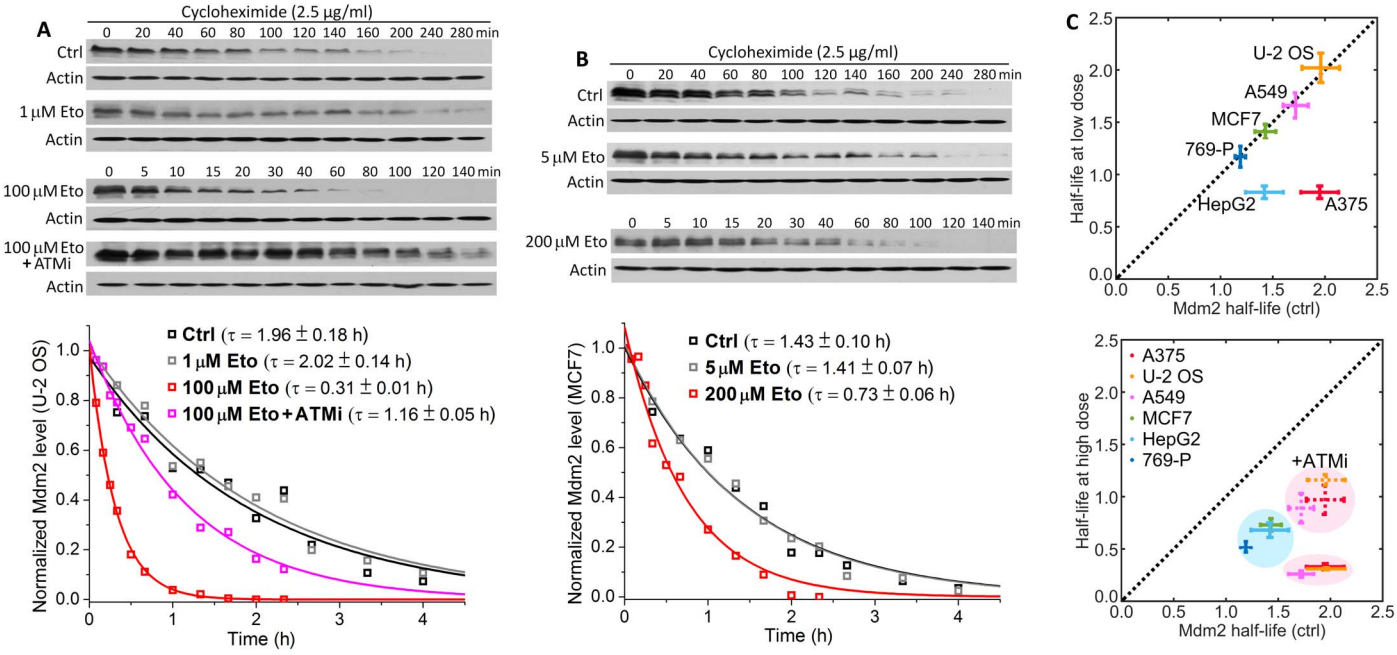

Fig. 3. Dose-dependent Mdm2 expression was mainly regulated by ATM-mediated Mdm2 degradation. (**A**) Mdm2 degradation kinetics in U-2 OS cells under the indicated treatment condition plus cycloheximide (2.5 μg/ml) were measured by Western blot analysis of Mdm2 level at 12 selected time points (unit: minute). Actin, which served as a loading control, was shown beneath each Mdm2 sample. Mdm2 half-life τ under different treatment conditions was derived from the exponential fit of the Mdm2 degradation kinetics averaged from three independent sets of Western blots. (**B**) Mdm2 degradation kinetics of MCF7 cells and the respective exponential fits under the indicated treatment conditions. (**C**) Mdm2 half-life of the six cell lines at low (top) or high (bottom) drug dose in comparison with that under the control condition. The bottom panel also showed Mdm2 half-life of the three sensitive lines under the combined treatment of 100 μM etoposide and 20 μM KU55933, an ATM inhibitor (ATMi). ctrl, control.

and p53. Dynamics of this model are governed by the following delay differential equations (DDEs)

$$\frac{d[\mathrm{p53}]}{dt} = k_{\mathrm{p0}} - k_{\mathrm{mp}}\left([\mathrm{ATM_p}], [\mathrm{Wip1}]\right)[\mathrm{p53}][\mathrm{Mdm2}] - \gamma_{\mathrm{p}}[\mathrm{p53}] \quad (1)$$

$$\frac{d[\mathrm{Mdm2}]}{dt} = k_{\mathrm{m0}} + \frac{k_{\mathrm{pm}}[\mathrm{p53}]^{n_{\mathrm{m}}}_{t-\tau_{\mathrm{m}}}}{K^{n_{\mathrm{m}}}_{\mathrm{pm}}\left([\mathrm{ATM_p}]_{t-\tau_{\mathrm{m}}}, [\mathrm{Wip1}]_{t-\tau_{\mathrm{m}}}\right) + [\mathrm{p53}]^{n_{\mathrm{m}}}_{t-\tau_{\mathrm{m}}}} - \gamma_{\mathrm{m}}\left([\mathrm{ATM_p}], [\mathrm{Wip1}], \gamma_{m0}, \gamma_{m1}\right)[\mathrm{Mdm2}] \quad (2)$$

$$\frac{d[\mathrm{Wip1}]}{dt} = k_{\mathrm{w0}} + \frac{k_{\mathrm{pw}}[\mathrm{p53}]^{n_{\mathrm{w}}}_{t-\tau_{\mathrm{w}}}}{K^{n_{\mathrm{w}}}_{\mathrm{pw}}\left([\mathrm{ATM_p}]_{t-\tau_{\mathrm{w}}}, [\mathrm{Wip1}]_{t-\tau_{\mathrm{w}}}\right) + [\mathrm{p53}]^{n_{\mathrm{w}}}_{t-\tau_{\mathrm{w}}}} - \gamma_{\mathrm{w}}[\mathrm{Wip1}] \quad (3)$$

$$\frac{d[\mathrm{ATM_p}]}{dt} = S_{\mathrm{ea}}[\mathrm{Eto}]\left(\mathrm{ATM_t} - [\mathrm{ATM_p}]\right) - D_{\mathrm{a0}}[\mathrm{ATM_p}] \quad (4)$$

where "[]" denotes dimensionless concentrations of the total proteins (p53, Mdm2, and Wip1) or the active form of ATM (phospho-ATM, denoted by $\mathrm{ATM_p}$). The equations were derived using the rapid equilibrium assumption to simplify the phosphorylation and dephosphorylation of p53 and Mdm2 (see the Supplementary Materials for detailed derivation of the equations). k_{p0}, k_{m0}, and k_{w0} are the basal production rates of p53, Mdm2, and Wip1, respectively. The p53-induced production rates of Mdm2 and Wip1 are characterized by a Hill function, where τ_{m} and τ_{w} are the respective time delays in Mdm2 and Wip1 production. Moreover, we assume a linear basal degradation of p53, Mdm2, and Wip1, while Mdm2-mediated degradation of p53 is described by a second-order reaction with a rate constant, k_{mp}. γ_{m0} and $\gamma_{\mathrm{m1}}$are the degradation rates of unphosphorylated and phosphorylated Mdm2, respectively. The total concentration of ATM, $[\mathrm{ATM_t}] = [\mathrm{ATM_u}] + [\mathrm{ATM_p}]$, is considered a constant. Given that ATM and Wip1 can change the stability of p53 and Mdm2 and the transcriptional activity of p53, k_{mp}, K_{pm}, K_{pw}, and γ_{m} are taken as functions of [ATM] and [Wip1] (see the Supplementary Materials for the expression of these coefficients). To simulate the DDEs for the two different cell lines, we selected parameter values based on the Western blot results of U-2 OS and MCF7 (tables S1 and S2). In particular, U-2 OS cells were set to have a higher level of total ATM, while MCF7 cells had higher levels of Mdm2 and Wip1.

The simulation of the four-component model produced the same cell line–specific bimodal p53 dynamics as observed in the single-cell imaging experiments (Fig. 4, A and B). At low drug dose, p53 oscillation was activated in both U-2 OS and MCF7 cells. Under high etoposide concentration, the steady-state p53 level in U-2 OS cells was high, while the p53 level in MCF7 only rose slightly (Fig. 4C). Hence, p53 tended to return to a low level after transient elevation, resulting in an extended large pulse. On the basis of the model, we next computationally investigated the quantitative dependence of p53 dynamics on ATM, Mdm2, and Wip1 at high drug dose, where the sensitive U-2 OS and resistant MCF7 differed. To distinguish the dynamics of monotonic increase and

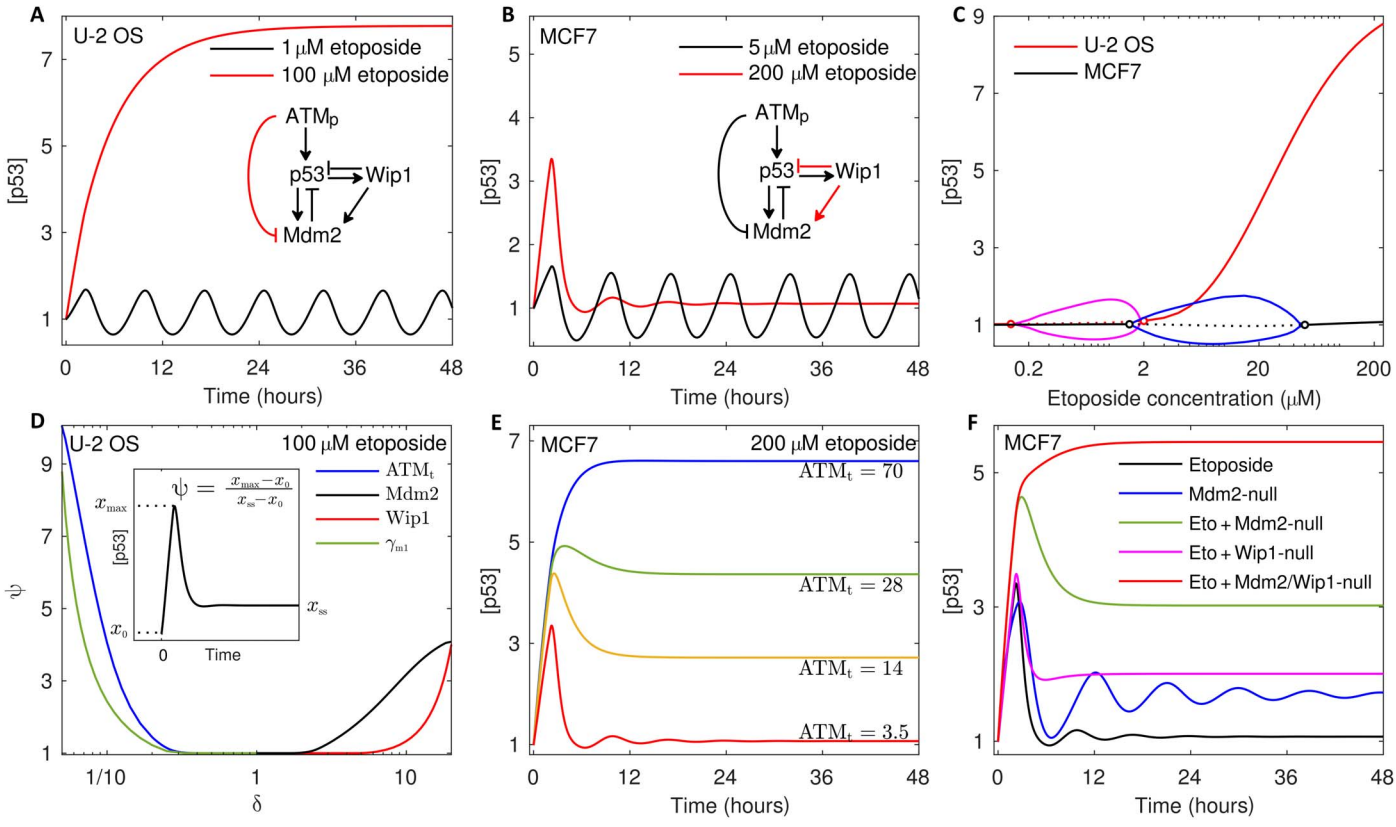

Fig. 4. Bimodal p53 dynamics were regulated by a four-component regulatory module consisting of ATM, p53, Mdm2, and Wip1. (**A** and **B**) Simulated single-cell dynamics of p53 and the corresponding four-component module. The black and red trajectories are p53 levels as a function of time under 1 μM (5 μM) and 100 μM (200 μM) etoposide in (A) U-2 OS and (B) MCF7 cells, respectively. (**C**) Bifurcation diagram of p53 concentration versus etoposide concentration. The red and black curves denote the respective steady states for U-2 OS and MCF7 cells. The solid and dotted curves separately denote the stable and unstable states. The circles denote the Hopf bifurcation points. The magenta (blue) curves denote the maxima and minima of [p53] in the limit cycles for U-2 OS (MCF7) cells. The *x* axis is on log scale. (**D**) Dependence of p53 induction dynamics in U-2 OS cell on expression of ATM_t, Mdm2, and Wip1 and the ATM-mediated Mdm2 degradation rate γ_{m1}. The above parameters were either increased or decreased by δ-fold. (**E**) Effects of total amount of ATM on p53 dynamics in MCF7 at 200 μM etoposide. (**F**) Simulated p53 dynamics in MCF7 cells under the indicated treatment conditions: 200 μM etoposide (black), Mdm2 inhibition (blue), 200 μM etoposide + Wip1 inhibition (magenta), 200 μM etoposide + Mdm2 inhibition (green), and 200 μM etoposide + combined inhibition of Mdm2 and Wip1 (red).

an extended large pulse, we defined a quantity ψ as follows to quantify the degree to which p53 dynamics resemble a typical large pulse

$$\psi = \frac{x_{max} - x_0}{x_{ss} - x_0} \quad (5)$$

As shown in the inset of Fig. 4D, x_0 is the initial level of p53 (i.e., steady-state value without drug treatment), x_{max} is the maximal p53 level induced by etoposide, and x_{ss} is the steady-state level of p53 under drug treatment. Note that ψ = 1 when p53 dynamics are monotonically increased and ψ > 1 for an extended large pulse. A larger ψ corresponds to p53 dynamics with a stronger resemblance to a typical large pulse. We first simulated p53 dynamics for U-2 OS cell under the perturbations of total ATM (i.e., $[ATM_t]$ in the equations), Mdm2 (i.e., k_{m0} and k_{pm}), and Wip1 (i.e., k_{w0} and k_{pw}), as well as the rate of ATM-mediated Mdm2 autodegradation (i.e., γ_{m1}), by increasing or decreasing the values of the respective parameters by δ-fold (Fig. 4D). Simulation results show that reducing the level of total ATM or ATM activity in catalyzing Mdm2 degradation and increasing the expression of Mdm2 or Wip1 could all change the p53 dynamics of U-2 OS cells from a monotonic increase to an extended large pulse, indicating that these are viable routes to evolve drug resistance. Comparatively, reducing the total ATM expression had the greatest effect on altering p53 dynamics to the suppressive large-pulse mode at the same fold change of value, indicating that ATM expression likely exerts the strongest control over the dynamic output of the ATM/p53/Mdm2/Wip1 regulatory module, and down-regulation of ATM expression is a highly effective way to dampen p53 induction and thus engender drug resistance.

Next, we simulated how p53 dynamics can be altered from an extended large pulse to monotonic induction in MCF7 cells (Fig. 4, E and F). Considering that monotonic p53 induction activates extensive etoposide-induced cell death, changing large p53 pulses to monotonic increases may be an effective way to enhance the cell death response of the resistant cell lines. As expected, increasing the total ATM can change p53 dynamics from a large pulse to a monotonic increase in MCF7 (Fig. 4E). The inhibition of Mdm2 activity had a notable effect on prolonging the duration of the p53 pulse and increasing the steady-state level of p53 at high drug dose, but p53 dynamics remained an extended large pulse (Fig. 4F). The removal of Wip1 alone did not significantly affect p53 dynamics, illustrating that Wip1 is dispensable for generating a large p53 pulse (e.g., as observed for 769-P). It was only under the simultaneous

inhibition of Mdm2 and Wip1 that p53 dynamics changed from a large pulse to monotonic induction in MCF7 under high drug dose. Overall, these results indicated that, although both Mdm2 and Wip1 play an inhibitory role on p53 dynamics, the inhibitory strength exerted by Mdm2 is stronger than that by Wip1. In other words, Mdm2-p53 functions as the primary inhibitory negative feedback, while Wip1-p53 serves as a secondary inhibitory control that is critical only when Mdm2-p53 is inhibited or attenuated.

Alteration of p53 dynamics sensitized resistant cancer to apoptosis

To validate the modeling results regarding the control of p53 dynamics and to examine whether change of p53 dynamics can enhance cell death response of the resistant cell lines to etoposide, we performed single-cell imaging experiments under the treatment of 200 μM etoposide plus inhibition of Mdm2, Wip1, or both. We used Nutlin-3, a small-molecule inhibitor of Mdm2, to inhibit Mdm2 activity. Wip1 was removed by RNA interference (RNAi) knockdown. Knockdown efficiency was generally more than 90%, and Wip1 knockdown alone induced little cell death (<5%) up to 72 hours of experiment. As shown in Fig. 5A, the loss of Wip1 did not alter the large-pulse dynamics of p53 induction in MCF7 cells in response to high concentration of etoposide. Upon Mdm2 inhibition by Nutlin-3, p53 dynamics changed from a short pulse (duration of 8 to 12 hours) to a long pulse (duration of 18 to 25 hours), although the steady-state level of p53 was lower than that predicted by the model simulation. Strong, monotonic induction of p53 was observed in MCF7 under the combinatorial treatment of Nutlin-3, Wip1 knockdown, and 200 μM etoposide, confirming the simulation results. Moreover, we found that the change of p53 dynamics to monotonic induction significantly enhanced and accelerated etoposide-induced cell death (Fig. 5B). Compared with less than 10% MCF7 cell death after a 36-hour treatment of etoposide alone, the monotonically increasing p53 engendered by the triple treatment triggered more than 80% cell death for the same time duration, illustrating that altering p53 dynamics is sufficient to sensitize MCF7 cells to etoposide-induced cell death and that Mdm2 and Wip1 are viable combinatorial targets to enhance the response of resistant cancers to DNA-damaging drugs. The other two resistant cell lines, HepG2 and 769-P, also exhibited a similar change of p53 dynamics and a significant increase of cell death, with the combined inhibition of Mdm2 and Wip1 (Fig. 5C). Moreover, we found that attenuating ATM activity in the three sensitive cell lines, i.e., A375, U-2 OS, and A549, by RNAi knockdown of ATM altered their p53 dynamics from more than 75% monotonic induction to about 60% pulsing (both periodic pulsing and extended large pulse) in response to high concentration of etoposide (fig. S6), and this change toward pulsing p53 reduced etoposide-induced cell death from more than 75% to about 40% in the three sensitive lines. These data further confirmed the key role of ATM activity in regulating p53 dynamics and that p53 pulsing promoted cell cycle arrest and chemoresistance.

In addition, further Western blot analysis of MCF7 cells showed that Wip1 knockdown strongly enhanced p53 phosphorylation, e.g., at Ser^{15} and Ser^{46}, and moderately reduced Mdm2 expression, but did not affect the phosphorylation level of ATM (Fig. 5D). Phosphorylation of p53 at Ser^{15} is known to stabilize p53 (*10*, *27*), and phosphorylation at Ser^{46} particularly activates the proapoptotic target genes of p53 (*28*–*30*). Therefore, the Wip1-p53 negative feedback likely attenuates p53 induction by simultaneously destabilizing p53 and stabilizing Mdm2 and also decreases the cell death response to etoposide by mitigating p53's transcriptional activation of proapoptotic genes.

DISCUSSION

Our study not only elucidates a new dynamic mechanism underlying resistance to DNA-damaging drugs, but also provides new insight to understanding cell type–dependent variability in p53 pathway–mediated DNA damage response. Variation in cell death response to cytotoxic chemotherapy is possibly the most crucial factor that distinguishes the sensitive and resistant tumors, as clinical response of tumor regression or delay in tumor growth often correlates with the cell death response (*31*, *32*). Our data show that the dynamic mode of p53 activation, especially at regimes of high concentrations of DNA-damaging drugs, determines the sensitivity of p53-wild-type cancers to drug-induced cell death. In the resistant cancer cells that we studied, the dynamic output is dampened mainly by attenuating Mdm2 inhibition by ATM due to either down-regulation of ATM expression or reduced ATM binding/activity toward Mdm2. Our modeling results further showed that perturbation of other modular features, such as overexpression of Mdm2 or Wip1 (*33*), could also promote p53 pulsing and drug resistance. For a broader spectrum of tumor types, additional regulatory components and interactions in a larger p53 pathway beyond this four-component core module could also be involved. Although the precise molecular mechanisms that contribute to p53 pulsing upon drug treatment may differ, our data point to the combinatorial inhibition of Mdm2 and Wip1 as a promising strategy to change p53 dynamics from pulsing to monotonic induction and combat this dynamic chemoresistance.

The fact that we found that the down-regulation of ATM reduced the cellular sensitivity to DNA-damaging drugs puts a cautious note on combining ATM inhibitors with DNA-damaging chemotherapeutics for cancer treatment (*34*). The loss of ATM activity was first found to sensitize cells to ionizing radiation (IR), sparking the interest to develop ATM inhibitors as anticancer drugs, particularly as a combinatorial therapy with IR and DNA-damaging drugs (*35*). Early data showed tumor cells with defective p53 were more pronouncedly sensitized by ATM inhibitors to IR and chemo drugs (*36*), while a recent study concluded that the sensitizing effect was significant in both p53 wild-type and p53-deficient cells (*37*). It remains unclear whether and how the functional status of p53 affects response to ATM inhibitors. Our study showed that the attenuation of ATM activity desensitizes, rather than sensitizes, the response of p53 wild-type cancer cells to DNA-damaging drugs. Although the down-regulation of ATM activity may not give rise to exactly the same phenotypic response as that of complete inhibition of the kinase, our results do argue against combining ATM inhibitors with chemo drugs for tumors with wild-type p53.

By investigating a large range of DNA damage doses, we characterized p53 activation dynamics and drug response at a dynamical regime that is more associated with cell death. The typical etoposide dose applied to patients is 100 mg/m^2 per day, which results in a peak plasma drug concentration of approximately 20 μg/ml, i.e., 34 μM (*38*). As shown in Fig. 1E, this dose level of etoposide is sufficient to activate monotonic p53 induction and cell death in >80% of A375 and U-2 OS cells, suggesting that their dose responses are possibly informative of sensitive tumors in the clinical context. At the same dose level, less than 5% cell death was induced in the resistant lines, validating them as models of resistant cancer. The resistance mechanism that we elucidated for the three resistant cancer lines thus may help to guide the identification of some resistant tumors. Less clear is how normal cells respond to etoposide at this treatment dosage. For the cytotoxic therapy to work, a favorable efficacy-to-toxicity ratio ("therapeutic index") has to be achieved, i.e., the drug needs to kill tumors without killing the

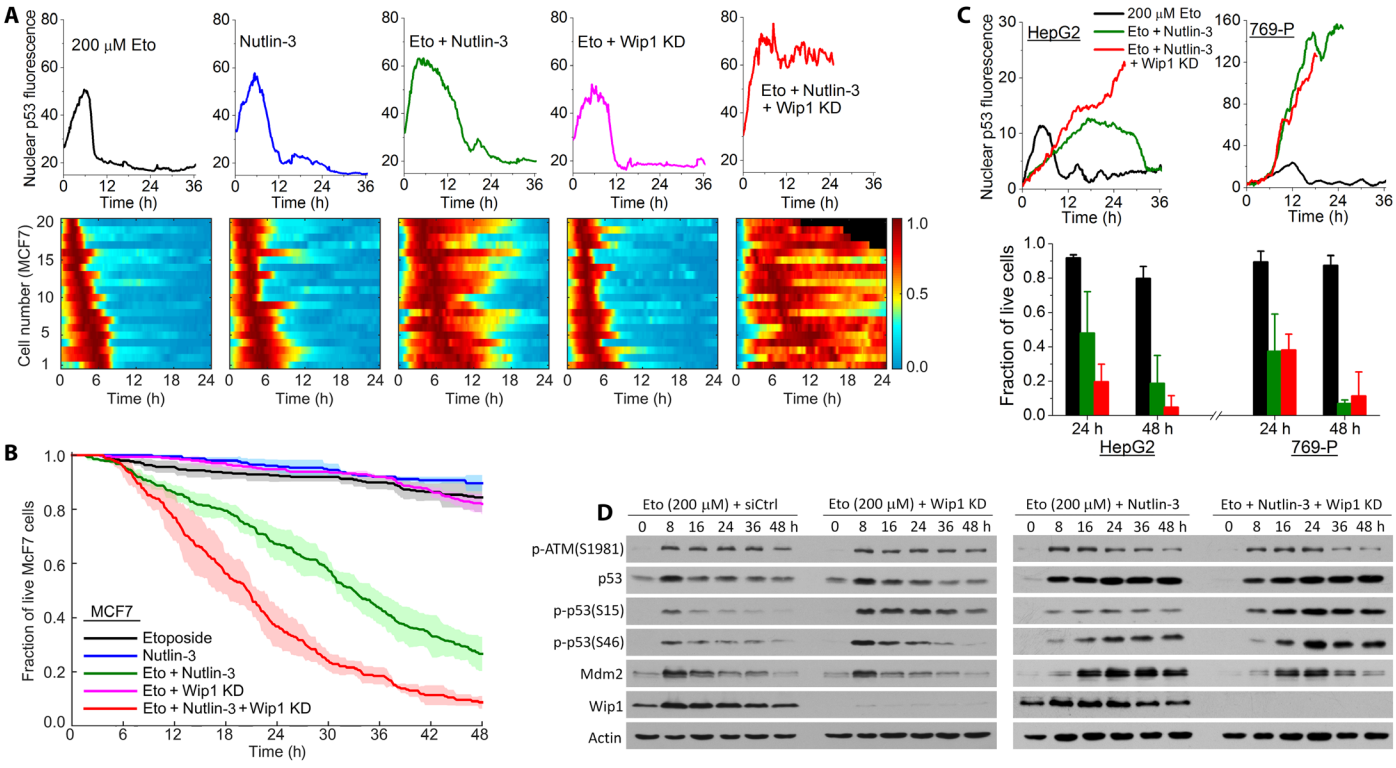

Fig. 5. Inhibition of Mdm2 or Mdm2 plus Wip1 altered p53 dynamics in the resistant cell lines and sensitized their drug-induced cell death. (**A**) Representative single-cell trajectories and heat maps of p53-Venus fluorescence in individual MCF7 cells under the indicated treatment conditions, including etoposide (200 μM) alone, Nutlin-3 (10 μM) alone, etoposide + Nutlin-3, etoposide + Wip1 knockdown (KD), and etoposide + Nutlin-3 + Wip1 KD. Cells under treatment conditions without Wip1 knockdown were transfected with nontargeting small interfering RNA (siRNA) to control for transfection toxicity. The abrupt end of p53 trajectory and the black squares in the heat map under etoposide + Nutlin-3 + Wip1 KD correspond to the time of death. (**B**) Cumulative survival curves of MCF7 cells under the indicated treatment conditions. Data were averaged from three independent imaging experiments, and the total number of cells analyzed for each condition in each experiment ranged from 62 to 132. Cell death was scored morphologically on the basis of time-lapse movies, and the kinetics of cell death were plotted as cumulative survival curves. The shaded area of each curve indicates SD. (**C**) Representative single-cell p53 trajectories of HepG2 and 769-P cells and their survival statistics after 24 or 48 hours of the indicated treatment conditions. Data were averaged from two independent imaging experiments, and the total number of cells analyzed for each condition in each experiment ranged from 40 to 129. (**D**) Western blot comparison of selected proteins/protein modifications of MCF7 cells treated with 200 μM etoposide plus control siRNA or Wip1 KD or 200 μM etoposide + 10 μM Nutlin-3 versus etoposide + Nutlin-3 + Wip1 KD.

patient. Normal cells obviously have wild-type p53, and our results suggest that retraining p53 dynamics to the pulsing mode protects cells from drug-induced cell death. We do not yet know how the regulatory module that controls p53 dynamics differs between normal and cancer cells and whether it is possible to develop a combinatorial target that can achieve a better therapeutic index, e.g., by protecting normal cells or sensitizing cancer to respond to a lower drug dose. Nonetheless, our results point to the modulation of p53 activation dynamics as a new possible angle to explore new drug targets and drug combinations.

On the basic biology of signaling molecule dynamics and pathway control, our data provide new evidence that a major function of p53 pulsing, both in the form of periodic pulsing and an extended large pulse, is to suppress p53 induction level and its activity to trigger cell death. Periodic pulsing of p53 dynamics has been extensively investigated before, with most studies attributing it to a time-delayed negative feedback loop between p53 and Mdm2 (*39*). The dynamic mode of a large p53 pulse was also previously analyzed for response to transient UV radiation and was attributed to differential activation of Wip1 (*18*). However, our results showed that Wip1 did not play a significant role in engendering a large p53 pulse in the model system that we studied. Both experimental and computational analysis of the ATM/p53/Mdm2/Wip1 regulatory module showed that attenuation of the positive feed-forward loop of ATM-Mdm2-p53 is the key to generating a large p53 pulse at high DNA damage. It appears that mechanisms that activate even the same p53 dynamic mode may differ, depending on the stimulus. To unravel how the regulatory module that controls p53 dynamics may be differentially activated in a stimulus-dependent manner, we will need to investigate and compare single-cell p53 dynamics in response to a wider variety of stress stimuli, such as nucleolar stress and hypoxia, in follow-up studies.

MATERIALS AND METHODS

Cell culture

Cell lines were purchased from the American Type Culture Collection (USA) and cultured under 37°C and 5% CO_2 in an appropriate medium supplemented with 10% fetal calf serum (FCS), penicillin (100 U/ml), and streptomycin (100 μg/ml). A375 was maintained in Dulbecco's modified Eagle's medium, U-2 OS in McCoy's 5A (modified) medium, A549 in F-12K medium, MCF7 and 769-P in RPMI 1640 medium, and HepG2 in minimum essential medium. To generate fluorescent reporter cells for live-cell imaging analysis of p53 dynamics, we infected

the individual cell lines with lentiviruses encoding an established p53-Venus reporter and selected isogenic clones that exhibited dose responses most similar to their respective parental line for conducting the study. The p53-Venus reporter construct, consisting of wild-type p53 fused to a yellow fluorescent protein, Venus, was a gift from G. Lahav at the Department of Systems Biology, Harvard Medical School.

Chemicals and reagents

Etoposide, Nutlin-3, and the ATM kinase inhibitors KU55933 and KU60019 were purchased from Tocris or Selleckchem. siRNA oligos for gene knockdown include siWip1 (UUGGCCUUGUGCCUACUAA; used at a final concentration of 20 nM), sip53 (UGAACCAUUGUUCAAUAUCGUCCGG; used at 20 nM), and siATM-1 (GCCUCCAGGCAGAAAAAGA; used at 40 nM in A375 and A549. This oligo was a gift from M. Huen [School of Biomedical Sciences, University of Hong Kong (*40*)], and siATM-2 (used at 60 nM in U-2 OS; #sc-29761, Santa Cruz Biotechnology). Dharmacon On-Target plus siControl (#D-001810-01) was used as a nontargeting siRNA control. siRNA transfections were performed in U-2 OS cells using HiPerFect (Qiagen), and in all other cell lines using Lipofectamine (Thermo Fisher Scientific) according to the manufacturer's instructions. Experiments were conducted after 48 hours of gene silencing.

Time-lapse microscopy

Cells were plated in a 24-well glass-bottom imaging plate (Cellvis, USA) and cultured in a phenol red–free CO_2-independent medium (Invitrogen) supplemented with 10% FCS, penicillin (100 U/ml), and streptomycin (100 μg/ml). Cell images were acquired with a Nikon TE2000-PFS inverted microscope enclosed in a humidified chamber maintained at 37°C. Cells were imaged every 10 min using a motorized stage and a 20× objective (numerical aperture, 0.95).

For data plotted in Figs. 1 and 5, we viewed and analyzed the images manually to determine the drug response phenotypes using the MetaMorph software (Molecular Dynamics). We scored cell fate by morphological tracking as follows: interphase (by flat morphology), entry into mitosis (by cell rounding), cell division (by respreading and splitting), cell cycle arrest (by absence of cell division for 72 hours), and cell death (by blebbing followed by cell lysis). The dynamic mode of nuclear p53 was scored on the basis of the p53-Venus fluorescence in the nucleus. To quantify the single-cell p53 trajectories, we used an automatic cell tracking program that we developed using MATLAB. The program consists of image analysis procedures that sequentially segment the individual cells, track them in time, identify the nucleus, and measure the p53 fluorescence intensity in the nucleus.

Western blot analysis

Cell lysates were obtained using a lithium dodecyl sulfate sample buffer (NuPAGE, Invitrogen). Proteins were resolved on 8 to 15% tris-glycine gels and transferred onto polyvinylidene difluoride membranes. Blots were probed with commercially available primary antibodies and chemiluminescent detection using ECL Prime (Amersham). Antibodies such as Parp1 (#9542), phospho-p53 (S15) (#9284), ATM (#2873), phospho-Chk2 (Thr^{68}) (#2197), p21 (#2947), and Puma (#4976) were purchased from Cell Signaling Technology; p53 (#sc-126), Mdm2 (#sc-965), and Wip1 (#sc-20712) from Santa Cruz Biotechnology; γH2A.X (#06-570) from Millipore; and phospho-ATM (S1981) (#ab81292) and phospho-p53 (S46) (#ab76242) from Abcam. Anti-actin (#A5316) from Sigma-Aldrich was used as a loading control.

Mathematical model and computational analysis

Detailed description of the four-component model of the core p53 regulatory module and computational analysis of this model in terms of differential activation of bimodal p53 dynamics in response to variable DNA damage signals can be found in Results and the Supplementary Materials.

SUPPLEMENTARY MATERIALS

Supplementary material for this article is available at http://advances.sciencemag.org/cgi/content/full/4/12/eaat5077/DC1

Supplementary Text

Table S1. Model parameters for U-2 OS cells.

Table S2. Model parameters for MCF7 cells.

Fig. S1. p53 dependence of cell death response induced by etoposide (topoisomerase inhibitor) and doxorubicin (DNA intercalator).

Fig. S2. Single-cell trajectories of p53 dynamics from the six cell lines in response to high dose of etoposide.

Fig. S3. Quantification of Western blot comparison of the six cell lines shown in Fig. 2E.

Fig. S4. Inhibitory effect of KU55933 on ATM activation.

Fig. S5. Mdm2 degradation kinetics and the derived Mdm2 half-life τ of A375, A549, HepG2, and 769-P.

Fig. S6. Effects of ATM knockdown on promoting p53 pulsing and attenuating cell death of the three sensitive cell lines in response to high concentration of etoposide.

REFERENCES AND NOTES

1. S. V. Sharma, D. W. Bell, J. Settleman, D. A. Haber, Epidermal growth factor receptor mutations in lung cancer. *Nat. Rev. Cancer* **7**, 169–181 (2007).
2. P. Karran, Mechanisms of tolerance to DNA damaging therapeutic drugs. *Carcinogenesis* **22**, 1931–1937 (2001).
3. S. P. Jackson, J. Bartek, The DNA-damage response in human biology and disease. *Nature* **461**, 1071–1078 (2009).
4. D. W. Meek, Tumour suppression by p53: A role for the DNA damage response? *Nat. Rev. Cancer* **9**, 714–723 (2009).
5. K. H. Vousden, D. P. Lane, p53 in health and disease. *Nat. Rev. Mol. Cell Biol.* **8**, 275–283 (2007).
6. J. M. Gudas, H. Nguyen, T. Li, L. Sadzewicz, R. Robey, K. Wosikowski, K. H. Cowan, Drug-resistant breast cancer cells frequently retain expression of a functional wild-type p53 protein. *Carcinogenesis* **17**, 1417–1427 (1996).
7. S. C. Righetti, G. Della Torre, S. Pilotti, S. Ménard, F. Ottone, M. I. Colnaghi, M. A. Pierotti, C. Lavarino, M. Cornarotti, S. Oriana, S. Böhm, G. L. Bresciani, G. Spatti, F. Zunino, A comparative study of *p53* gene mutations, protein accumulation, and response to cisplatin-based chemotherapy in advanced ovarian carcinoma. *Cancer Res.* **56**, 689–693 (1996).
8. M. Martinez-Rivera, Z. H. Siddik, Resistance and gain-of-resistance phenotypes in cancers harboring wild-type p53. *Biochem. Pharmacol.* **83**, 1049–1062 (2012).
9. C. Dai, W. Gu, p53 post-translational modification: Deregulated in tumorigenesis. *Trends Mol. Med.* **16**, 528–536 (2010).
10. J.-P. Kruse, W. Gu, Modes of p53 regulation. *Cell* **137**, 609–622 (2009).
11. J. E. Chipuk, T. Kuwana, L. Bouchier-Hayes, N. M. Droin, D. D. Newmeyer, M. Schuler, D. R. Green, Direct activation of Bax by p53 mediates mitochondrial membrane permeabilization and apoptosis. *Science* **303**, 1010–1014 (2004).
12. K. H. Vousden, C. Prives, Blinded by the light: The growing complexity of p53. *Cell* **137**, 413–431 (2009).
13. X. Chen, J. Chen, S. Gan, H. Guan, Y. Zhou, Q. Ouyang, J. Shi, DNA damage strength modulates a bimodal switch of p53 dynamics for cell fate control. *BMC Biol.* **11**, 73 (2013).
14. J. E. Purvis, K. W. Karhohs, C. Mock, E. Batchelor, A. Loewer, G. Lahav, p53 dynamics control cell fate. *Science* **336**, 1440–1444 (2012).
15. G. Lahav, N. Rosenfeld, A. Sigal, N. Geva-Zatorsky, A. J. Levine, M. B. Elowitz, U. Alon, Dynamics of the p53-Mdm2 feedback loop in individual cells. *Nat. Genet.* **36**, 147–150 (2004).
16. E. Batchelor, C. S. Mock, I. Bhan, A. Loewer, G. Lahav, Recurrent initiation: A mechanism for triggering p53 pulses in response to DNA damage. *Mol. Cell* **30**, 277–289 (2008).
17. A. Loewer, E. Batchelor, G. Gaglia, G. Lahav, Basal dynamics of p53 reveal transcriptionally attenuated pulses in cycling cells. *Cell* **142**, 89–100 (2010).
18. E. Batchelor, A. Loewer, C. Mock, G. Lahav, Stimulus-dependent dynamics of p53 in single cells. *Mol. Syst. Biol.* **7**, 488 (2011).
19. J. Stewart-Ornstein, G. Lahav, p53 dynamics in response to DNA damage vary across cell lines and are shaped by efficiency of DNA repair and activity of the kinase ATM. *Sci. Signal.* **10**, eaah6671 (2017).

20. J. L. Nitiss, Targeting DNA topoisomerase II in cancer chemotherapy. *Nat. Rev. Cancer* **9**, 338–350 (2009).
21. A. A. Cohen, N. Geva-Zatorsky, E. Eden, M. Frenkel-Morgenstern, I. Issaeva, A. Sigal, R. Milo, C. Cohen-Saidon, Y. Liron, Z. Kam, L. Cohen, T. Danon, N. Perzov, U. Alon, Dynamic proteomics of individual cancer cells in response to a drug. *Science* **322**, 1511–1516 (2008).
22. S. L. Spencer, S. Gaudet, J. G. Albeck, J. M. Burke, P. K. Sorger, Non-genetic origins of cell-to-cell variability in TRAIL-induced apoptosis. *Nature* **459**, 428–432 (2009).
23. D. Michael, M. Oren, The p53–Mdm2 module and the ubiquitin system. *Semin. Cancer Biol.* **13**, 49–58 (2003).
24. X. Le Guezennec, D. V. Bulavin, WIP1 phosphatase at the crossroads of cancer and aging. *Trends Biochem. Sci.* **35**, 109–114 (2010).
25. A. Lindqvist, M. de Bruijn, L. Macurek, A. Brás, A. Mensinga, W. Bruinsma, O. Voets, O. Kranenburg, R. H. Medema, Wip1 confers G2 checkpoint recovery competence by counteracting p53-dependent transcriptional repression. *EMBO J.* **28**, 3196–3206 (2009).
26. J. M. Stommel, G. M. Wahl, Accelerated MDM2 auto-degradation induced by DNA-damage kinases is required for p53 activation. *EMBO J.* **23**, 1547–1556 (2004).
27. F. Toledo, G. M. Wahl, Regulating the p53 pathway: In vitro hypotheses, in vivo veritas. *Nat. Rev. Cancer* **6**, 909–923 (2006).
28. M. Takekawa, M. Adachi, A. Nakahata, I. Nakayama, F. Itoh, H. Tsukuda, Y. Taya, K. Imai, p53-inducible Wip1 phosphatase mediates a negative feedback regulation of p38 MAPK-p53 signaling in response to UV radiation. *EMBO J.* **19**, 6517–6526 (2000).
29. K. Oda, H. Arakawa, T. Tanaka, K. Matsuda, C. Tanikawa, T. Mori, H. Nishimori, K. Tamai, T. Tokino, Y. Nakamura, Y. Taya, *p53AIP1*, a potential mediator of p53-dependent apoptosis, and its regulation by Ser-46-phosphorylated p53. *Cell* **102**, 849–862 (2000).
30. N. Taira, K. Nihira, T. Yamaguchi, Y. Miki, K. Yoshida, DYRK2 is targeted to the nucleus and controls p53 via Ser46 phosphorylation in the apoptotic response to DNA damage. *Mol. Cell* **25**, 725–738 (2007).
31. W. F. Symmans, M. D. Volm, R. L. Shapiro, A. B. Perkins, A. Y. Kim, S. Demaria, H. T. Yee, H. McMullen, R. Oratz, P. Klein, S. C. Formenti, F. Muggia, Paclitaxel-induced apoptosis and mitotic arrest assessed by serial fine-needle aspiration: Implications for early prediction of breast cancer response to neoadjuvant treatment. *Clin. Cancer Res.* **6**, 4610–4617 (2000).
32. T. Ni Chonghaile, K. A. Sarosiek, T.-T. Vo, J. A. Ryan, A. Tammareddi, V. Del Gaizo Moore, J. Deng, K. C. Anderson, P. Richardson, Y.-T. Tai, C. S. Mitsiades, U. A. Matulonis, R. Drapkin, R. Stone, D. J. DeAngelo, D. J. McConkey, S. E. Sallan, L. Silverman, M. S. Hirsch, D. R. Carrasco, A. Letai, Pretreatment mitochondrial priming correlates with clinical response to cytotoxic chemotherapy. *Science* **334**, 1129–1133 (2011).
33. D. V. Bulavin, O. N. Demidov, S. Saito, P. Kauraniemi, C. Phillips, S. A. Amundson, C. Ambrosino, G. Sauter, A. R. Nebreda, C. W. Anderson, A. Kallioniemi, A. J. Fornace Jr., E. Appella, Amplification of *PPM1D* in human tumors abrogates p53 tumor-suppressor activity. *Nat. Genet.* **31**, 210–215 (2002).
34. A. M. Weber, A. J. Ryan, ATM and ATR as therapeutic targets in cancer. *Pharmacol. Ther.* **149**, 124–138 (2015).
35. A. M. R. Taylor, D. G. Harnden, C. F. Arlett, S. A. Harcourt, A. R. Lehmann, S. Stevens, B. A. Bridges, Ataxia telangiectasia: A human mutation with abnormal radiation sensitivity. *Nature* **258**, 427–429 (1975).
36. S. N. Powell, J. S. DeFrank, P. Connell, M. Eogan, F. Preffer, D. Dombkowski, W. Tang, S. Friend, Differential sensitivity of $p53^{(-)}$ and $p53^{(+)}$ cells to caffeine-induced radiosensitization and override of G_2 delay. *Cancer Res.* **55**, 1643–1648 (1995).
37. M. A. Batey, Y. Zhao, S. Kyle, C. Richardson, A. Slade, N. M. B. Martin, A. Lau, D. R. Newell, N. J. Curtin, Preclinical evaluation of a novel ATM inhibitor, KU59403, in vitro and in vivo in p53 functional and dysfunctional models of human cancer. *Mol. Cancer Ther.* **12**, 959–967 (2013).
38. K. R. Hande, P. J. Wedlund, R. M. Noone, G. R. Wilkinson, F. A. Greco, S. N. Wolff, Pharmacokinetics of high-dose etoposide (VP-16-213) administered to cancer patients. *Cancer Res.* **44**, 379–382 (1984).
39. N. Geva-Zatorsky, N. Rosenfeld, S. Itzkovitz, R. Milo, A. Sigal, E. Dekel, T. Yarnitzky, Y. Liron, P. Polak, G. Lahav, U. Alon, Oscillations and variability in the p53 system. *Mol. Syst. Biol.* **2**, 2006.0033 (2006).
40. Y. Guo, W. Feng, S. M. H. Sy, M. S. Y. Huen, ATM-dependent Phosphorylation of the Fanconi anemia protein PALB2 promotes the DNA damage response. *J. Biol. Chem.* **290**, 27545–27556 (2015).

Acknowledgments: We thank G. Lahav (Department of Systems Biology, Harvard Medical School) for the p53-Venus lentiviral vector and M. Huen (School of Biomedical Sciences, University of Hong Kong) for the siRNA oligo targeting ATM. **Funding:** This work was supported by the Hong Kong Research Grant Council (#N_HKBU215/13 and #T12-710/16-R) to J.S. and the National Science Foundation of China (#31361163003) to F.L. **Competing interests:** The authors declare that they have no competing interests. **Author contributions:** J.S. and F.L. designed the study. J.S. supervised the study. R.Y., Y.Z., and Y.L. performed the experiments. B.H. performed the computational analysis. R.Y., B.H., and J.S. analyzed the data. J.S., B.H., R.Y., and F.L. wrote the paper. **Data and materials availability:** All data needed to evaluate the conclusions in the paper are present in the paper and/or the Supplementary Materials. Additional data related to this paper may be requested from the authors.

Submitted 6 March 2018
Accepted 19 November 2018
Published 19 December 2018
10.1126/sciadv.aat5077

Citation: R. Yang, B. Huang, Y. Zhu, Y. Li, F. Liu, J. Shi, Cell type–dependent bimodal p53 activation engenders a dynamic mechanism of chemoresistance. *Sci. Adv.* **4**, eaat5077 (2018).